Synchronous Opening and Closing Motions are Essential for cAMP-Dependent Protein Kinase A Signaling

Atul K. Srivastava[1], Leanna R. McDonald[1], Alessandro Cembran[2], Jonggul Kim[2], Larry R. Masterson[2], Christopher L. McClendon[3], Susan S. Taylor[3], and Gianluigi Veglia[1,2]

[1]Department of Biochemistry, Molecular Biology and Biophysics, University of Minnesota, MN, 55455 United States.

[2]Department of Chemistry, University of Minnesota, Minnesota, 55455 United States.

[3]Department of Chemistry and Biochemistry, University of California at San Diego, La Jolla, CA 92093, USA

SUPPLEMENTARY INFORMATION

Supplementary Materials and Methods

NMR Spectroscopy. The T_1 experiments were acquired with relaxation delays of 10(x2), 100, 200, 300, 500, 700, 900, 1200, 1500 and 1700 ms. For $T_1\rho$ measurements, a spin-lock field strength of 1.5 kHz centered at the ^{15}N carrier frequency was used with spin-lock pulse on for 6(x2), 12, 18, 24, 30, 36, 48, 60, and 78 ms. T_1 and $T_1\rho$ values were calculated by fitting signal intensities to a single-exponential decay, and errors were estimated from the repeats of single data points. $T_1\rho$ values were converted into T_2 as described previously,

$$\mathrm{R}_{1\rho} = \mathrm{R}_1 (\cos\theta)^2 + \mathrm{R}_2 (\sin\theta)^2$$

$$\theta = \tan^{-1}\frac{\omega_1}{\Omega}$$

where R_1 and R_2 are the longitudinal and transverse relaxation rate constants, respectively. And is the tilt angle between the static magnetic field and the effective field. The spin-lock field strength (in frequency units) is $_1$, and is the resonance offset from the carrier frequency.

^{15}N[^{1}H]-NOE values were determined as the ratio of signal intensities from experiments performed with and without ^{1}H saturation for 4 s. Errors in the ^{15}N[^{1}H]-NOE were calculated via error propagation using root mean square noise of the spectra. R_{ex} was measured using the TROSY-Hahn-echo method with a Hahn-echo period of $2/J_{NH}$ (10.8 ms). Peak intensities were used to determine R_{ex} as described elsewhere (Wang et al., 2003).

$$R_{\mathrm{ex}} \cong C_{zz} \ln \rho_{\mathrm{zz}} + C_{\beta} \ln \rho_{\beta}$$

where $C_{zz} = (2\tau)^{-1}$, $C_{\beta} = (\kappa - 1) \times (4\tau)^{-1}$, $\kappa = 1 - 2 \times \ln\rho_{zz}/\ln\rho_{\beta}$, $\rho_{zz} = I_{zz}/I_{\alpha}$ and $\rho_{\beta} = I_{\beta}/I_{\alpha}$. The intensities of the spin states α, β and zz (I_{α}, I_{b} and I_{zz}) were obtained from the sum of four two-dimensional experiments. The value κ was determined from the trimmed mean of signal intensities of amides resonances not showing chemical exchange. Errors in R_{ex} were estimated by error propagation using root mean square noise of the spectra.

^{15}N TROSY-CPMG experiments were acquired with constant relaxation time of 40 ms with τ_{cp} delays of 10.00 (x2), 5.00, 3.33, 2.50, 1.67 (x2), 1.26, 1.00, 0.84, 0.72, 0.62, 0.56, and 0.50(x2) ms where τ_{cp} is the spacing between consecutive 180° pulses. ^{15}N TROSY-CPMG experiment was acquired on 800 and 900 MHz spectrometers with identical τ_{cp} values.

The relaxation dispersion data were analyzed with two-site exchange model using the all-timescales multiple quantum (M Q) Carver-Richards-Jones formulation which gets simplified to single quantum if $\Delta\omega_{H}$ is set zero. All the analysis of relaxation dispersion data was done using cpmg_fit (provided by Dr. Lewis Kay and Dr. Dmitry Korznev). The best fitting was selected using chi-square values. For fitting the following equation is used:

$$R_2^{eff} = R_2^0 + \frac{k_{ex}}{2} - v_{cpmg}\, cosh^{-1}\left[D_+ \cosh(\eta_+) - D_- \cosh(\eta_-)\right]$$ (Richard-Carver equation)

where

$$D_{\pm} = \frac{1}{2}\left[\pm 1 + \frac{\psi + 2\,\delta\omega^2}{(\psi^2 + \xi^2)^{1/2}}\right]$$

$$\eta_{\pm} = \frac{\left[\pm\psi + \left(\psi^2 + \xi^2\right)^{1/2}\right]^{1/2}}{2\sqrt{2}\, v_{cpmg}}$$

$$\psi = k_{ex}^2 - \delta\omega^2$$

$$\xi = -2\delta\omega\ (p_a k_{ex} - p_b k_{ex})$$

The populations (p_{closed}) and k_{ex} thus obtained were used to calculate the rate constants for the forward and backward rate constants, k_f and k_b using the following identities:

$$p_{closed} + p_{open} = 1\ ,$$

$$k_{ex} = k_f + k_b,$$

Molecular Dynamics Simulations.

System Preparation. Starting from the PKA-C in the closed state with ATP and two Mn^{2+} ions (PDB ID:3FJQ), the Protein Local Optimization Program was used to pre-process the PDB file (Jacobson et al., 2004). The structure was then imported into Maestro (Schrodinger, Inc.). The Mn^{2+} ions were changed to Mg^{2+} ions, and the Protein Preparation Wizard was used to assign bond orders, add hydrogens, and keep all crystal waters. Hydrogen bonds and histidine protonation states were optimized for neutral pH, yielding HIP for H87, HIE for H142, and HID protonation states for the remaining histidines. The crystal waters and PKI peptide were removed. Removal of Mg1 yielded the intermediate state with ATP and one Mg^{2+} bound. The protonation state of C199 was modeled as negatively charged based on the very high *in vitro* reactivity of this cysteine (Jimenez et al., 1982; Nelson and Taylor, 1981). The Y204A enzyme system was modeled as described above. The Y204 side chain was removed past the Cβ. Hydrogens were removed from both models before preparation for AMBER 11 (Case et al., 2011) and AMBER 12 (Case et al., 2012), using the FF99SB-ildn-nmr force field (Hornak et al., 2006; Li and Bruschweiler, 2010; Lindorff-Larsen et al., 2010). The proteins were solvated in a cubic box of

TIP4P-EW water (Horn et al., 2004) with 10 Å buffers, with parameters for ATP (Meagher et al., 2003), phosphothreonine (Homeyer et al., 2006), and phosphoserine (Homeyer et al., 2006) taken from the Bryce group's AMBER Parameter Database (Bryce). SHAKE (Ryckaert et al., 1977) was used to constrain all covalent bonds from to hydrogen atoms.

Molecular Dynamics Simulations. The program AMBER12 was used for the initial energy-minimization, heating, and equilibration steps, using the pmemd.cuda module (Gotz et al., 2012; Le Grand et al., 2013). Each system was energy-minimized, first with position restraints on the protein and ATP/Mg^{2+}, and then without restraints. Constant volume simulations using particle mesh Ewald (Darden et al., 1993). The range-limited cutoff was dropped to 8 Å (the long-ranged electrostatics are moved into the Ewald terms) and the equilibration was continued for 50ns.

Molecular dynamics simulations with a 2 fs time step were performed to heat the systems from 0 K to 300 K, linearly over 500ps, with 10.0 kcal/mol/Å position restraints on the protein and ATP/Mg^{2+}. Temperature was maintained by the Langevin thermostat, with a collision frequency of 1 ps^{-1}. Then constant pressure dynamics was performed with isotropic position scaling; initially with position restraints for 100 ps and a relaxation time of 2 ps, and then without position restraints for 100 ps. The range-limited cutoff was dropped to 8 Å and the simulation was continued for 50 ns. For Y204A, an additional 50 ns was run at constant volume. Each system was simulated briefly for 12 ps of Nosé-Hoover constant volume MD (Hoover, 1985; Nose, 1984) using Desmond (DE Shaw Research) at 2 fs time steps to further prepare for simulation on Anton. Production runs for closed/ATP/two Mg^{2+}, closed/ATP/one Mg^{2+}, and open/ATP/one Mg^{2+} were performed on a 512-node Anton supercomputer at constant volume, using time steps of 2 fs and the Nosé-Hoover thermostat (Hoover, 1985; Nose, 1984) with a relaxation time of 1 ps and center of mass motion removed. The wild-type system was simulated for 5.7 microseconds and the Y204A system was simulate for 5.1 microseconds. Trajectories were aligned by the C-lobe. The "g_chi" module of GROMACS was used to extract dihedral angles, noting that

GROMACS reports backbone dihedrals using a slightly nonstandard definition, where the amide hydrogen and oxygen in one residue are used to define these dihedrals without referring to atoms in other residues.

FIGURE S1, related to Table 1

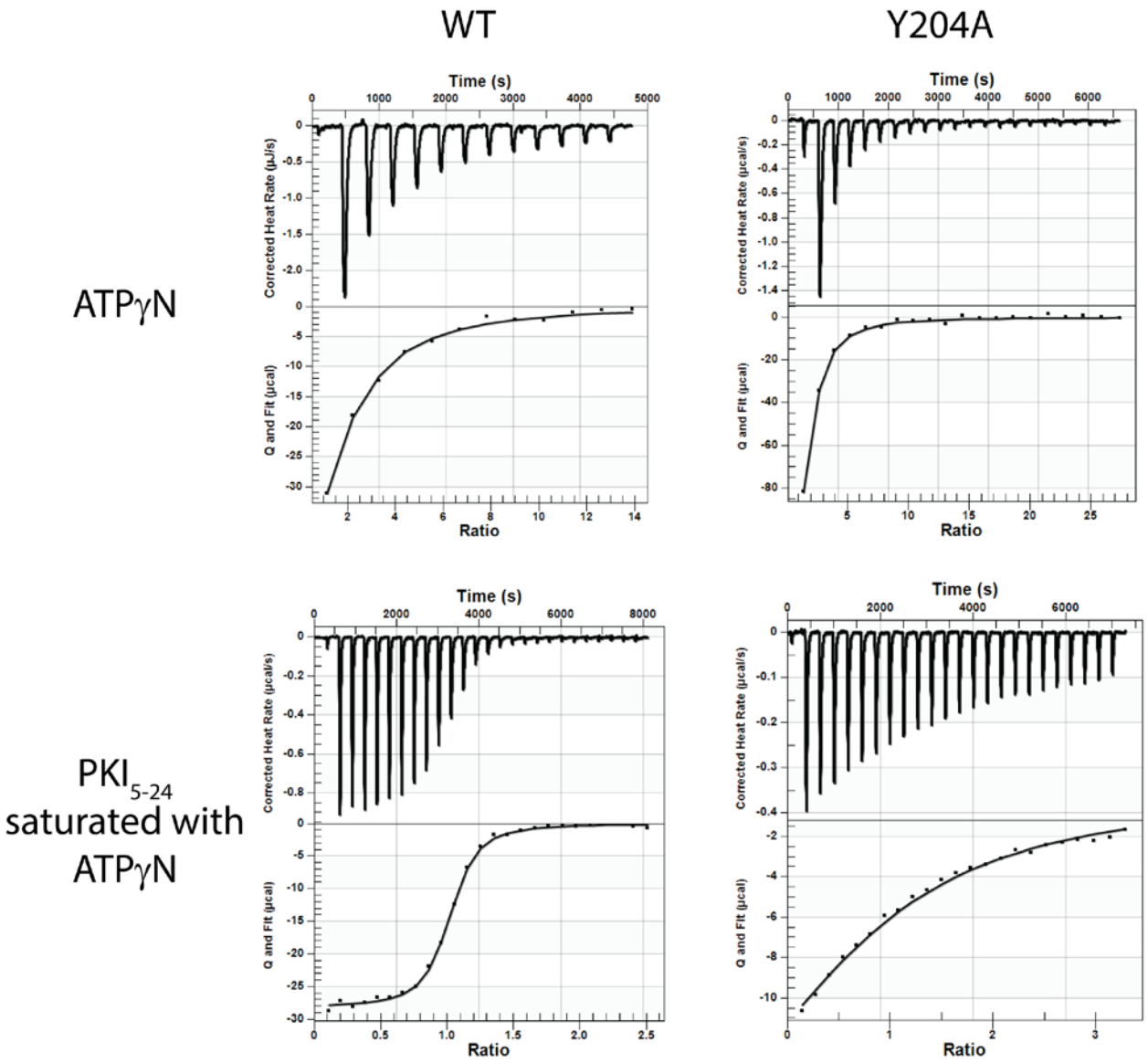

Figure S1: Isothermal Titration Calorimetry (ITC) with ATPγN to the apo form and the pseudo-substrate PKI_{5-24} to the ATPγN-bound form of PKA-C^{WT} and PKA-C^{Y204A}. Top: ATPγN binding to Apo PKA-C^{WT} and the PKA-C^{Y204A} mutant. Bottom: Pseudo-substrate, PKI_{5-24}, binding to PKA-C^{WT} and PKA-C^{Y204A} in the presence of 2 mM ATPγN. All measurements were performed in triplicate and the error reflects the standard deviation.

FIGURE S2, related to Figure 2

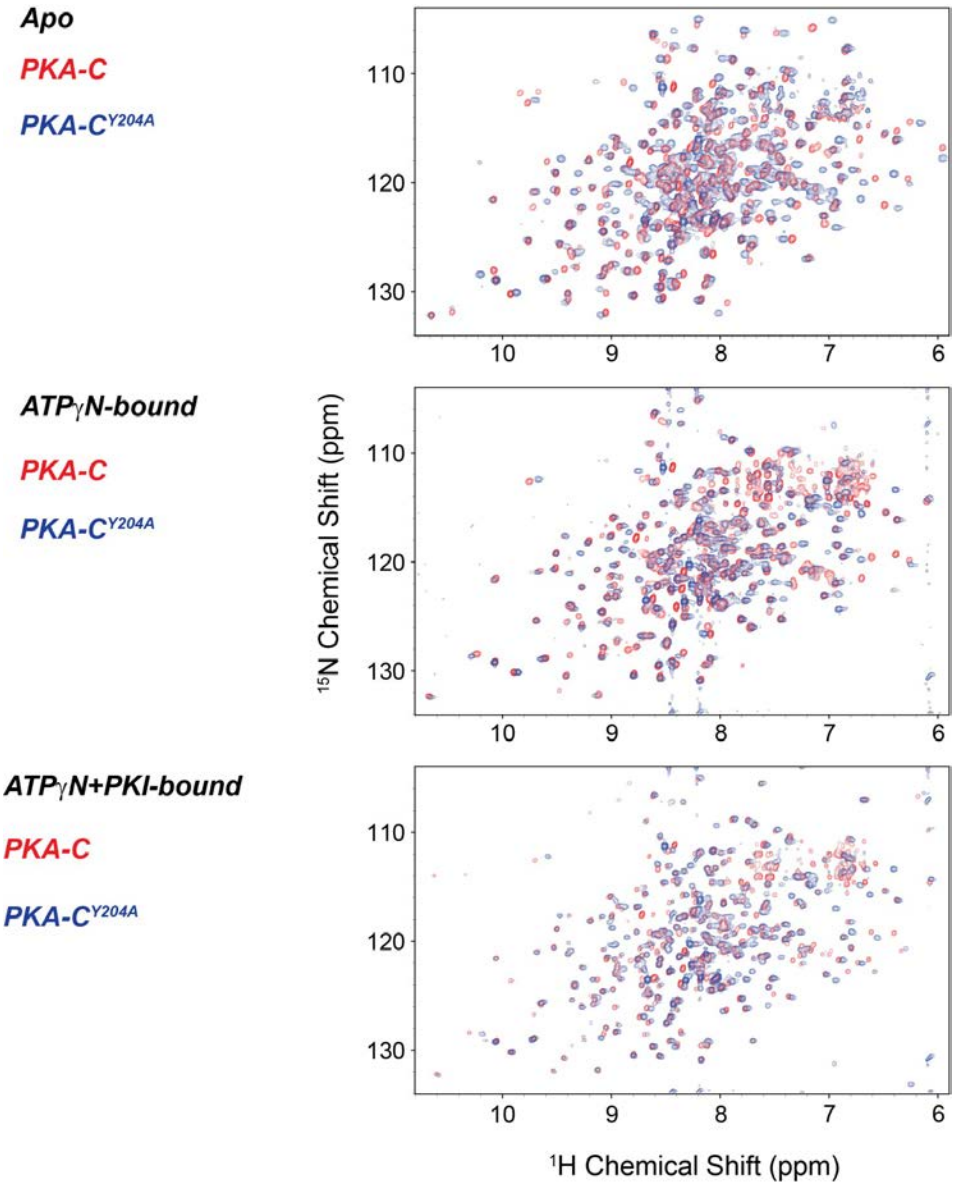

Figure S2: Overlays of the [^{1}H, ^{15}N]-TROSY-HSQC spectra for PKA-C^{WT} and PKA-C^{Y204A} for the three forms of the kinase: apo (top), ATPγN-bound (middle), and ATPγN and PKI$_{5-24}$-bound (bottom).

FIGURE S3, related to Figure 2

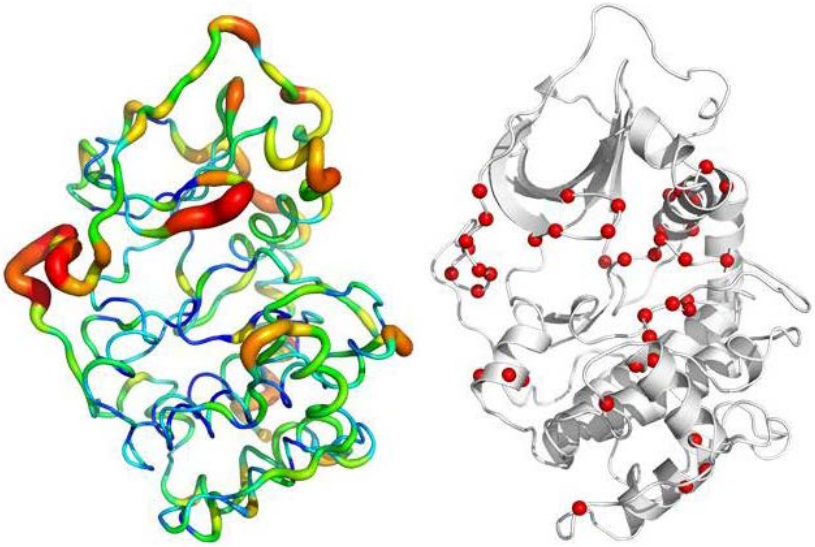

Figure S3: Qualitative comparison of the B-factor from the crystal structure 1BKX (left) with the resonances undergoing broadening beyond detection upon binding the nucleotide (also shown in Figure 2). B-factors are shown in a rainbow scale from blue (1) to red (100).

FIGURE S4, related to Figure 3

A4	A97	G214	W302
A5	N99	K217	A304
K7	V104	D220	K309
K8	S109	I228	E311
Q12	K111	A240	A312
K16	D112	D241	F314
K21	N113	Q245	F318
S34	S114	K254	K319
T37	N115	R256	E334
A38	Y117	F261	I335
Q39	S139	S262	R336
D41	E140	S263	V337
D44	H142	D267	I339
R45	A148	T278	N340
I46	I150	K279	E341
K47	D175	R280	K342
G55	Q176	N283	C343
K63	Q177	N286	K345
E64	Y179	G287	E346
N67	Q181	D290	
A70	K189	I291	
D75	R190	H294	
K76	G193	A298	
V79	E208	T299	
I94	L211	D301	

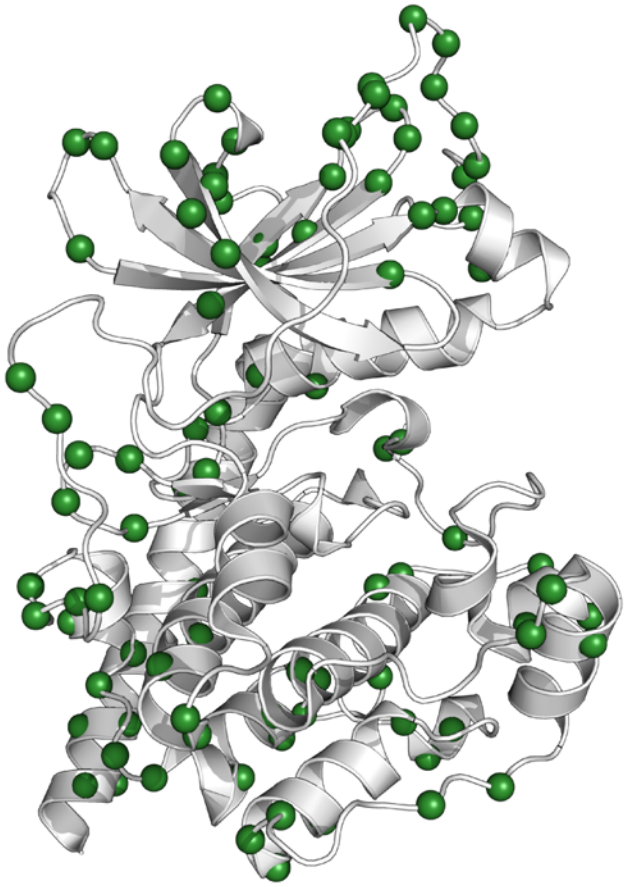

Figure S4. Left: List of residues that defined linear trajectories for the 6 states analyzed with CONCISE using the thresholds reported in the Methods section. Right: The linear residues are mapped onto the kinase structure (1ATP).

FIGURE S5, related to Table 1

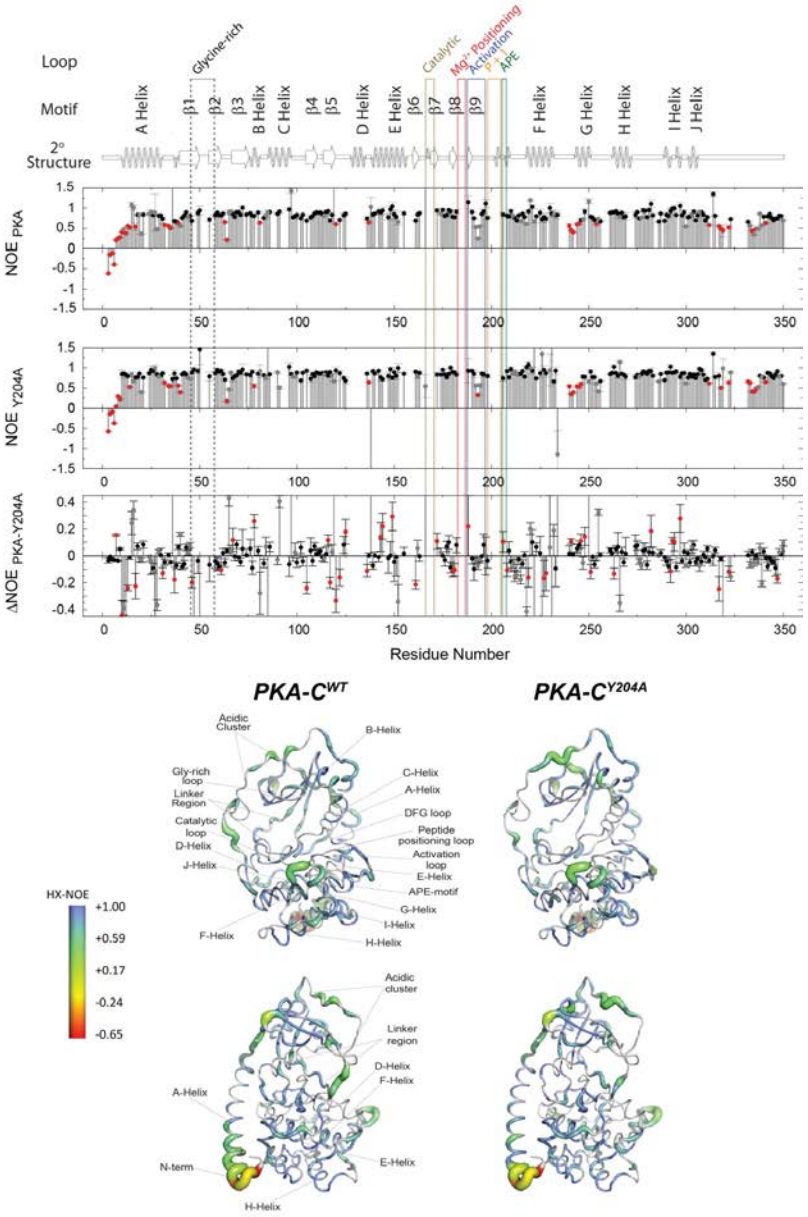

Figure S5: ^{1}H-^{15}N HX-NOE as probe of fast conformational dynamics. Top: The HX-NOE is plotted as a function of the PKA sequence where the red colored values represent NOEs above or below one standard deviation from the average. Bottom: HX-NOE values reported on the crystal structure 1ATP of the kinase. Bulges and colors show regions with higher mobility. S10, Q12, E13, E17, T37, I46, K61, K105 are more rigid in the mutant (higher values of HX-NOEs), while K7, N67, K78 are more dynamic (lower HX-NOE values). Residues near or belonging to the linker regions and preceding the D-helix (Y117, M120 and Y122) are relatively rigid; whereas G125, located near a C-spine residue, and A188, right after the DFG-loop, are more mobile. In the peptide positioning loop, A206 becomes rigid, while E208 becomes mobile in the Y204A enzyme.

FIGURE S6, related to Figure 6

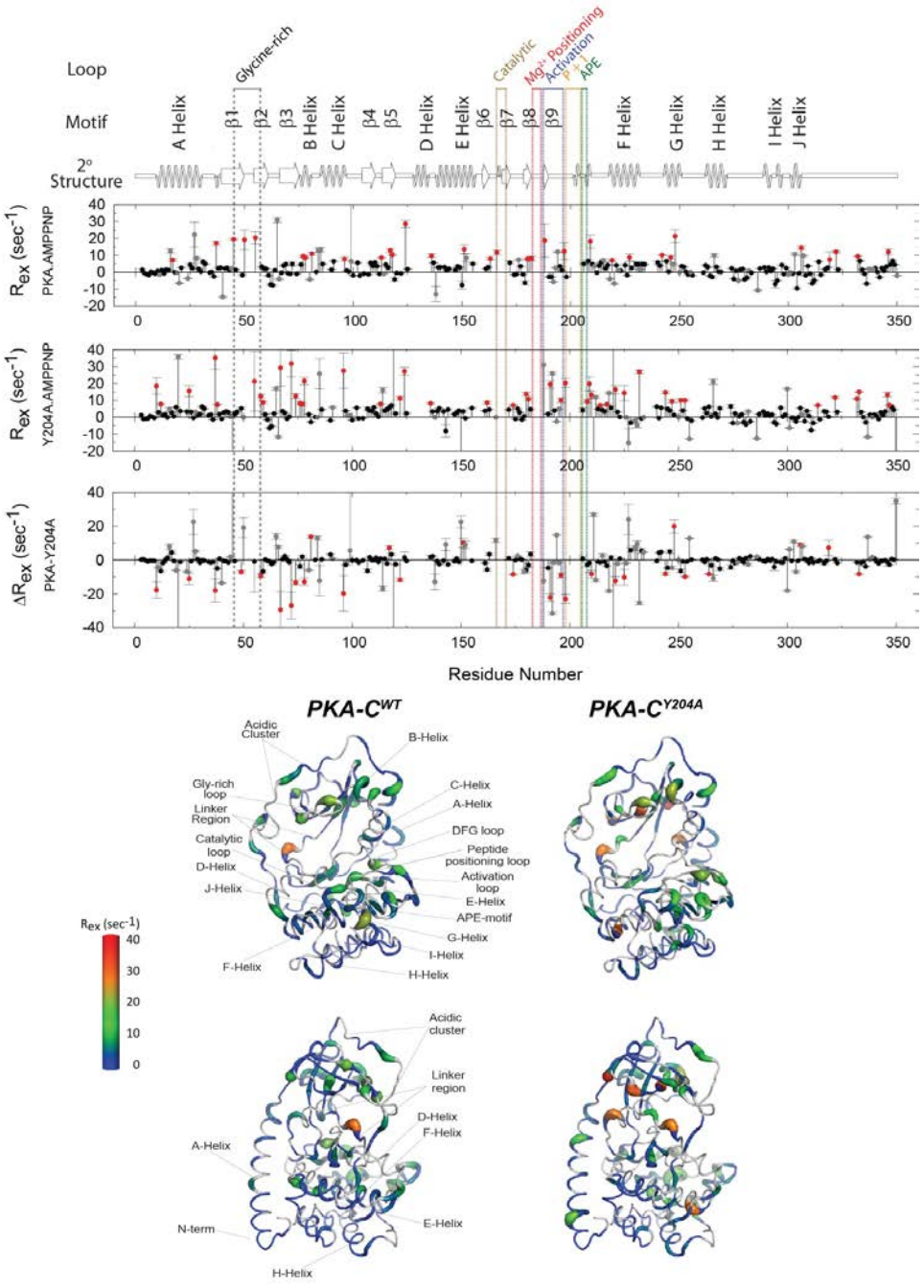

Figure S6: ^{15}N TROSY Hahn-echo as a probe for slow conformational dynamics. Top: R_{ex} values obtained from the TrHE experiments are plotted as a function of the PKA sequence where the red colored values represent $R_{ex} > 7$ s^{-1} and $|\Delta R_{ex}| > 7$ s^{-1}. Due to the magnitude and orientation of the ^{15}N chemical shift tensor, the R_{ex} values for the non-exchanging residues are scattered around zero with a standard deviation of approximately 2 s^{-1}. Bottom: R_{ex} values are shown on the crystal structure 1ATP of the kinase with bulges and colors highlighting the regions with higher mobility.

SUPPLEMENTARY TABLES

TABLE S1, related to Table 1: Thermodynamics of ligand binding to PKA-C^{WT} and PKA-C^{Y204A} determined by ITC. Binding of the ATP mimic, ATPγN, to Apo form of the enzyme (top) was measured as well as PKI_{5-24} binding of the nucleotide bound form of the enzyme (bottom).

ATPγN	**K_d (μM)**	**ΔH (kcal/mol)**	**TΔS (kcal/mol)**
PKA-C^{WT}	58 ± 4	-2.7 ± 0.2	3.1 ± 0.2
PKA-C^{Y204A}	23.5 ± 0.85	-4.25 ± 0.05	2.11 ± 0.03
PKI_{5-24} with 2mM ATPγN	**K_d (μM)**	**ΔH (kcal/mol)**	**TΔS (kcal/mol)**
PKA-C^{WT}	0.12 ± 0005	-18.1 ± 0.27	-8.64 ± 0.3
PKA-C^{Y204A}	14.6 ± 2.1	-8.57 ± 0.39	-1.92 ± 0.46

TABLE S2, related to Table 1. ^{15}N CPMG relaxation dispersion group fit of PKA-C^{WT}.

Residue	**Δω (ppm)**	**$R_2°$ (s^{-1}) 800 MHz**	**$R_2°$ (s^{-1}) 900 MHz**	**R_{ex} (s^{-1})* 800 MHz**	**R_{ex} (s^{-1})* 800 MHz**
55	1.28 ± 0.99	15.7 ± 1.7	17.3 ± 1.9	19.2 ± 9.5	22.7 ± 15.7
58	0.80 ± 0.52	13.4 ± 0.6	16.9 ± 0.5	8.8 ± 3.6	10.8 ± 2.5
59	0.52 ± 0.33	15.0 ± 0.6	17.0 ± 0.5	4.0 ± 3.1	5.0 ± 2.7
72	0.82 ± 0.54	15.0 ± 0.9	15.9 ± 0.9	9.1 ± 5.6	11.2 ± 5.3
77	0.72 ± 0.46	19.1 ± 0.6	19.9 ± 0.5	7.3 ± 3.1	9.0 ± 2.7
78	0.63 ± 0.40	12.9 ± 0.4	12.8 ± 0.4	5.7 ± 2.1	7.1 ± 2.0
91	0.73 ± 0.47	17.4 ± 0.7	18.3 ± 0.7	7.4 ± 3.7	9.1 ± 3.2
96	0.81 ± 0.54	17.6 ± 0.7	20.6 ± 0.7	9.1 ± 3.8	11.2 ± 3.9
124	1.02 ± 0.72	22.3 ± 1.1	26.9 ± 1.2	13.4 ± 6.6	16.2 ± 6.9
163	0.66 ± 0.42	15.6 ± 0.5	18.3 ± 0.5	6.2 ± 2.8	7.6 ± 2.5
181	0.82 ± 0.54	17.3 ± 0.8	19.1 ± 0.8	9.2 ± 4.5	11.3 ± 4.1
306	0.63 ± 0.40	14.6 ± 0.5	13.9 ± 0.5	5.7 ± 2.8	7.1 ± 2.3
318	0.43 ± 0.25	9.2 ± 0.3	10.1 ± 0.3	2.7 ± 0.6	3.4 ± 0.5
332	0.77 ± 0.50	13.6 ± 0.4	15.1 ± 0.4	8.2 ± 1.6	10.1 ± 1.5
346	0.75 ± 0.49	19.2 ± 0.8	20.0 ± 0.8	7.8 ± 5.0	9.7 ± 4.5

Group parameters: **k_{ex} = 1020 ± 150 s^{-1}, p_{closed} = 0.935 ± 0.085**
*Calculated from Carver-Richards equation and fit parameters.

TABLE S3, related to Figure 4. ^{15}N CPMG relaxation dispersion individual fit of PKA-C^{WT}.

Residue	k_{ex} (s^{-1})	Δω (ppm)	P_{closed}	$R_2°$(s^{-1}) 800 MHz	$R_2°$(s^{-1}) 900 MHz	R_{ex}(s^{-1})* 800 MHz	R_{ex}(s^{-1})* 900 MHz	χ^2
38	1700 ± 1100	0.66 ± 1.07	0.95 ± 0.21	13.1 ± 0.5	14.0 ± 0.5	3.3 ± 2.1	4.1 ± 2.6	2.77
49	3000 ± 1500	3.56 ± 0.51	0.991 ± 0.002	14.7 ± 1.2	22.3 ± 1.2	7.0 ± 1.0	8.3 ± 1.1	0.39
55[a]	780 ± 1100	2.07 ± 1.11	0.965 ± 0.014	15.1 ± 1.4	16.4 ± 1.8	17.7 ± 9.0	19.2 ± 9.9	0.42
58[a]	1300 ± 670	0.81 ± 1.05	0.93 ± 0.21	12.9 ± 0.7	16.5 ± 0.7	8.1 ± 4.3	10.1 ± 5.3	0.86
59[a]	890 ± 560	0.55 ± 0.73	0.94 ± 0.17	15.1 ± 0.5	16.9 ± 0.5	4.3 ± 2.4	5.4 ± 2.9	0.76
72[a]	550 ± 520	0.67 ± 0.97	0.93 ± 0.21	15.5 ± 0.9	16.6 ± 0.9	11.3 ± 7.6	13.4 ± 9.0	0.51
77[a]	18 ± 19	4.17 ± 0.55	0.77 ± 0.14	19.8 ± 1.9	20.8 ± 2.0	4.1 ± 1.5	4.1 ± 1.5	1.24
78[a]	890 ± 890	0.95 ± 2.02	0.97 ± 0.12	12.6 ± 0.4	12.4 ± 0.4	6.2 ± 5.1	7.4 ± 6.1	0.97
85	110 ± 150	7.84 ± 1.20	0.945 ± 0.074	16.9 ± 0.3	18.9 ± 0.3	6.2 ± 2.5	6.2 ± 2.5	0.26
91[a]	45 ± 79	3.21 ± 1.27	0.87 ± 0.18	17.1 ± 1.3	18.5 ± 1.3	5.9 ± 3.5	5.9 ± 3.5	0.33
96[a]	560 ± 240	0.60 ± 0.32	0.91 ± 0.10	18.2 ± 0.5	21.1 ± 0.5	11.8 ± 3.3	14.2 ± 4.0	0.37
118	2400 ± 2000	3.58 ± 1.83	0.995 ± 0.004	16.2 ± 0.7	15.0 ± 1.0	4.3 ± 1.5	4.9 ± 1.7	1.92
124[a]	1400 ± 1200	1.60 ± 2.43	0.965 ± 0.098	21.5 ± 1.0	25.7 ± 1.3	12.3 ± 7.8	14.6 ± 9.3	0.27
137	3300 ± 550	0.73 ± 0.06	0.887 ± 0.073	13.5 ± 0.3	12.4 ± 0.3	4.2 ± 0.3	5.3 ± 0.4	2.86
163[a]	470 ± 450	0.66 ± 0.96	0.95 ± 0.13	15.8 ± 0.4	18.6 ± 0.4	8.2 ± 5.3	9.6 ± 6.1	0.6
166	16 ± 27	2.39 ± 0.46	0.69 ± 0.28	22.1 ± 4.4	28.3 ± 4.5	5.0 ± 3.1	5.0 ± 3.1	0.44
172	20 ± 8.3	2.63 ± 0.63	0.813 ± 0.058	20.8 ± 0.8	19.9 ± 0.8	3.7 ± 0.7	3.7 ± 0.7	1.65
175	4200 ± 5800	8.69 ± 6.78	0.998 ± 0.001	9.2 ± 5.4	10.1 ± 6.3	5.1 ± 3.5	5.6 ± 3.9	0.66
180	2900 ± 4100	5.85 ± 3.02	0.995 ± 0.002	15.0 ± 3.9	14.8 ± 4.9	7.9 ± 4.3	8.8 ± 5.0	0.45
181[a]	590 ± 430	0.66 ± 0.74	0.92 ± 0.17	17.6 ± 0.8	19.8 ± 0.8	11.2 ± 5.8	13.5 ± 7.0	0.63
198	640 ± 670	0.36 ± 0.28	0.93 ± 0.14	13.6 ± 0.6	15.5 ± 0.6	3.4 ± 1.7	4.3 ± 2.2	1.34
231	1200 ±1500	0.49 ± 0.45	0.90 ± 0.27	18.7 ± 1.3	16.4 ± 1.3	4.7 ± 2.9	5.9 ± 3.7	0.44
242	3200 ± 3300	6.54 ± 2.61	0.995 ± 0.001	7.3 ± 3.9	10.9 ± 4.8	8.9 ± 4.4	9.9 ± 4.6	6.04
246	670 ± 660	0.77 ± 1.13	0.92 ± 0.24	19.3 ± 1.1	17.0 ± 1.1	13.5 ± 9.4	16.2 ± 11.3	0.69
248	22 ± 42	6.15 ± 1.40	0.62 ± 0.37	26.7 ± 7.7	26.8 ± 7.9	8.5 ± 6.4	8.5 ± 6.5	0.74
251	6700 ± 3500	0.91 ± 0.15	0.873 ± 0.084	17.6 ± 2.7	19.4 ± 2.9	3.3 ± 0.5	4.1 ± 0.6	1.88
306[a]	1600 ± 920	0.87 ± 1.78	0.95 ± 0.22	14.1 ± 0.4	13.3 ± 0.4	5.2 ± 3.7	6.4 ± 4.6	0.5
314	35 ± 89	5.64 ± 2.87	0.89 ± 0.21	14.0 ± 2.2	15.7 ± 2.2	3.7 ± 3.2	3.7 ± 3.2	4.08
318[a]	920 ± 420	0.52 ± 0.61	0.96 ± 0.10	9.2 ± 0.2	10.1 ± 0.2	2.8 ± 1.2	3.5 ± 1.5	2.46
332[a]	850 ± 640	0.79 ± 1.81	0.94 ± 0.25	13.8 ± 0.8	15.2 ± 0.7	8.7 ± 7.3	10.6 ± 8.9	1.69
346[a]	85 ± 170	1.23 ± 0.70	0.90 ± 0.16	19.6 ± 0.9	20.8 ± 0.9	8.1 ± 5.7	8.1 ± 5.7	0.63

Residues 37, 74, 136, 188, 240, 315, and 322 show significant dispersion, but are not included due to broad peaks leading to noisy data and imprecise fits.
*Calculated from Carver-Richards equation and fit parameters.
[a]Residues able to be group fit with parameters shown in Table S2.

TABLE S4, related to Figure 5. ^{15}N CPMG relaxation dispersion individual fit of PKA-C^{Y204A}.

Residue	k_{ex} (s^{-1})	Δω (ppm)	P_{closed}	$R_2°$(s^{-1}) 800 MHz	$R_2°$(s^{-1}) 900 MHz	$R_{ex}°$(s^{-1}) 800 MHz	$R_{ex}°$(s^{-1}) 900 MHz	χ^2
55	2700 ± 1100	1.12 ± 0.64	0.85 ± 0.27	16.3 ± 1.1	14.4 ± 1.1	14.5 ± 4.9	18.3 ± 6.3	0.24
58	1300 ± 2900	7.03 ± 2.97	0.997 ± 0.005	10.6 ± 1.6	12.4 ± 1.8	3.6 ± 2.6	3.7 ± 2.6	0.88
72	480 ± 680	1.02 ± 1.10	0.954 ± 0.056	18.5 ± 0.8	13.5 ± 0.8	12.1 ± 7.9	13.4 ± 8.8	0.66
77	20 ± 16	4.85 ± 0.48	0.78 ± 0.11	17.7 ± 1.5	20.3 ± 1.5	4.5 ± 1.2	4.5 ± 1.2	0.67
84	1700 ± 970	0.99 ± 1.97	0.95 ± 0.24	17.3 ± 0.6	17.8 ± 0.6	7.3 ± 5.2	9.1± 6.5	0.43
91	3100 ± 6400	8.14 ± 4.16	0.998 ± 0.001	11.6 ± 1.2	11.5 ± 1.2	4.2 ± 2.8	4.6 ± 3.0	1.21
96	750 ± 1100	1.36 ± 1.68	0.984 ± 0.026	17.6 ± 0.6	17.6 ± 0.7	5.4 ± 3.8	6.1 ± 4.3	0.5
124	2200 ± 1400	7.75 ± 1.20	0.993 ± 0.002	11.2 ± 0.8	14.9 ± 0.8	12.1 ± 2.6	12.7 ± 2.7	0.79
190	25 ± 22	2.57 ± 0.35	0.845 ± 0.11	11.5 ± 1.0	11.5 ± 1.0	3.7 ± 1.2	3.7 ± 1.2	1.91
198	31 ± 43	2.11 ± 0.45	0.80 ± 0.21	18.6 ± 2.3	20.5 ± 2.4	6.2 ± 3.1	6.2 ± 3.1	0.72
232	1900 ± 1600	2.78 ± 1.87	0.988 ± 0.014	18.0 ± 1.0	19.2 ± 1.4	8.5 ± 3.4	9.8 ± 4.0	2.48
332	1800 ± 550	0.75 ± 0.62	0.94 ± 0.12	11.1 ± 0.3	11.9 ± 0.3	4.3 ± 1.4	5.4 ± 1.7	0.91
333	210 ± 240	0.50 ± 0.31	0.913 ± 0.061	12.4 ± 0.4	10.1 ± 0.4	11.3 ± 5.3	12.4 ± 5.8	3.56
346	19 ± 30	2.46 ± 0.45	0.74 ± 0.26	20.0 ± 3.5	20.2 ± 3.6	4.9 ± 2.8	4.9 ± 2.8	1.16

Residues 74 and 181 show significant dispersion, but are not included due to broad peaks leading to noisy data and imprecise fits.
*Calculated from Carver-Richards equation and fit parameters.

REFERENCES

Bryce, R.A. AMBER parameter Database.

Case, D.A., Darden, T.A., Cheatham, T.E., III, Simmerling, C.L., Wang, J., Duke, R.E., Luo, R., Walker, R.C., Zhang, W., and Merz, K.M. (2011). Amber11. (University of California, San Francisco).

Case, D.A., Darden, T.A., Cheatham, T.E., III, Simmerling, C.L., Wang, J., Duke, R.E., Luo, R., Walker, R.C., Zhang, W., and Merz, K.M. (2012). Amber12. (University of California, San Francisco).

Darden, T., York, D., and Pedersen, L. (1993). Particle Mesh Ewald - an N.Log(N) Method for Ewald Sums in Large Systems. Journal of Chemical Physics *98*, 10089-10092.

Gotz, A.W., Williamson, M.J., Xu, D., Poole, D., Le Grand, S., and Walker, R.C. (2012). Routine Microsecond Molecular Dynamics Simulations with AMBER on GPUs. 1. Generalized Born. Journal of Chemical Theory and Computation *8*, 1542-1555.

Homeyer, N., Horn, A.H.C., Lanig, H., and Sticht, H. (2006). AMBER force-field parameters for phosphorylated amino acids in different protonation states: phosphoserine, phosphothreonine, phosphotyrosine, and phosphohistidine. J Mol Model *12*, 281-289.

Hoover, W.G. (1985). Canonical Dynamics - Equilibrium Phase-Space Distributions. Phys Rev A *31*, 1695-1697.

Horn, H.W., Swope, W.C., Pitera, J.W., Madura, J.D., Dick, T.J., Hura, G.L., and Head-Gordon, T. (2004). Development of an improved four-site water model for biomolecular simulations: TIP4P-Ew. The Journal of chemical physics *120*, 9665-9678.

Hornak, V., Abel, R., Okur, A., Strockbine, B., Roitberg, A., and Simmerling, C. (2006). Comparison of multiple Amber force fields and development of improved protein backbone parameters. Proteins *65*, 712-725.

Jacobson, M.P., Pincus, D.L., Rapp, C.S., Day, T.J., Honig, B., Shaw, D.E., and Friesner, R.A. (2004). A hierarchical approach to all-atom protein loop prediction. Proteins *55*, 351-367.

Jimenez, J.S., Kupfer, A., Gani, V., and Shaltiel, S. (1982). Salt-induced conformational changes in the catalytic subunit of adenosine cyclic 3',5'-phosphate dependent protein kinase. Use for establishing a connection between one sulfhydryl group and the gamma-P subsite in the ATP site of this subunit. Biochemistry *21*, 1623-1630.

Le Grand, S., Gotz, A.W., and Walker, R.C. (2013). SPFP: Speed without compromise-A mixed precision model for GPU accelerated molecular dynamics simulations. Comput Phys Commun *184*, 374-380.

Li, D.W., and Bruschweiler, R. (2010). NMR-based protein potentials. Angew Chem Int Ed Engl *49*, 6778-6780.

Lindorff-Larsen, K., Piana, S., Palmo, K., Maragakis, P., Klepeis, J.L., Dror, R.O., and Shaw, D.E. (2010). Improved side-chain torsion potentials for the Amber ff99SB protein force field. Proteins *78*, 1950-1958.

McClendon, C.L., Friedland, G., Mobley, D.L., Amirkhani, H., and Jacobson, M.P. (2009). Quantifying Correlations Between Allosteric Sites in Thermodynamic Ensembles. Journal of Chemical Theory and Computation *5*, 2486-2502.

McClendon, C.L., Hua, L., Barreiro, G., and Jacobson, M.P. (2012). Comparing Conformational Ensembles Using the Kullback-Leibler Divergence Expansion. Journal of Chemical Theory and Computation *8*, 2115-2126.

Meagher, K.L., Redman, L.T., and Carlson, H.A. (2003). Development of polyphosphate parameters for use with the AMBER force field. Journal of Computational Chemistry *24*, 1016-1025.

Morcos, F., Chatterjee, S., McClendon, C.L., Brenner, P.R., López-Rendón, R., John Zintsmaster, Maria Ercsey-Ravasz, Christopher R. Sweet, Matthew P. Jacobson, Jeffrey W. Peng*, et al.* (2010). Modeling conformational ensembles of slow functional motions in Pin1-WW. PLoS Computational Biology *in press*.

Nelson, N.C., and Taylor, S.S. (1981). Differential labeling and identification of the cysteine-containing tryptic peptides of catalytic subunit from porcine heart cAMP-dependent protein kinase. The Journal of biological chemistry *256*, 3743-3750.
Nose, S. (1984). A Unified Formulation of the Constant Temperature Molecular-Dynamics Methods. Journal of Chemical Physics *81*, 511-519.
Ryckaert, J.P., Ciccotti, G., and Berendsen, H.J.C. (1977). Numerical-Integration of Cartesian Equations of Motion of a System with Constraints - Molecular-Dynamics of N-Alkanes. J Comput Phys *23*, 327-341.
Wan, X., Ma, Y., McClendon, C.L., Huang, L.J., and Huang, N. (2013). Ab initio modeling and experimental assessment of Janus Kinase 2 (JAK2) kinase-pseudokinase complex structure. PLoS Computational Biology *9*, e1003022.
Wang, C.Y., Rance, M., and Palmer, A.G. (2003). Mapping chemical exchange in proteins with MW > 50 kD. Journal of the American Chemical Society *125*, 8968-8969.